Secondary shock wave in laser-material interaction

Sobieslaw Gacek and Xinwei Wang[a)]
Department of Mechanical Engineering, 2010 H. M. Black Engineering Building, Iowa State University, Ames, Iowa 50011-2161, USA

(Received 18 September 2008; accepted 22 October 2008; published online 16 December 2008)

In this work, the effects of shock driven process of the laser-ablated argon plume in a background gas environment are explored via molecular dynamics simulations. The primary shock wave propagation and its influence on the backward motion of the target material are delineated. It is observed that the strong pressure gradient inside the main shock wave overcomes the forward momentum of the plume and some compressed gas, leading to backward movement and redeposition on the target surface. Reflection of the backward moving gas on the target surface results in the secondary shock wave. Detailed investigation of the secondary shock wave phenomenon is provided, which gives, for the first time, an insight into formation and evolution of the internal gaseous shock at the atomistic level. © *2008 American Institute of Physics*.
[DOI: 10.1063/1.3039212]

In laser-material interaction the presence of background gas and the induced shock wave could significantly affect the dynamic behavior of the ablated plume.[1,2] In prominent research on the dynamics of laser ablation plume by Geohegan and Puretzky,[3] experimental investigation as well as theoretical study[4,5] of the plume splitting in low pressure background gases has been performed. Interesting theoretical study on gas dynamics of pulsed laser ablation by Han *et al.*[6] was conducted on shock wave formation in helium ambient gas and reflection of the shock front on a silicon substrate. Recent measurements of the internal structure and expansion dynamics of laser aluminum plumes have been reported in the work of Harilal *et al.*[7] Work by Singh *et al.*[8] provided study on the effect of ambient pressure on the redeposition of debris and the plume backward motion. Time-of-flight (TOF) signal oscillations according to generation of the primary and secondary shock wave in the plume-background gas interaction were observed in the experimental work by Bulgakov *et al.*,[9] and that exceptional feature has been covered empirically.[10]

There are a number of studies that have already examined laser ablation by molecular dynamics (MD) simulations. Profound work was performed by Zhigilei *et al.*[11] where a combined MD-Direct Simulation Monte Carlo Method computational model has been developed for simulation of the long-term plume expansion of organic systems. Of particular importance is the study conducted by Wang and Xu[12–14] and Wang.[15] The shock wave phenomenon has also received much attention and recently has been explored in near-field laser material interaction,[16] as well as its dynamic structure and mass penetration under picosecond laser irradiation.[17]

Although extensive experimental and theoretical work has been done on the shock wave in laser ablation, the formation of the secondary shock wave has not been explained satisfactorily. The objective of the present paper is to explicate the process of formation and particularly structure with thermodynamic and physical states of the secondary shock wave in nanoseconds range at molecular level.

Our current study shares the similar physical model as our established one, and the detailed description of the computational domain was given previously.[12–15,17] In brief, the physical target is placed in a gas environment and is irradiated by a laser pulse. The material is assumed to be argon crystal with an initial temperature of 50 K, where the background gas shares similar properties as the target, such as the molecular mass, but has a modified interatomic potential, which considers only repulsive force between atoms. The film target is 108 nm long in the z axis (direction of laser incidence), below which there is a gas domain 271 nm long. The computational domain measures $32.5\times2.7\times3627$ nm^3 $(x\times y\times z)$ and a total of 630 000 atoms is tracked in this case. Computational details along with parameter specifications are provided in other literatures.[12–18]

In our considerations, the spatial uniform single laser pulse irradiates the target top surface, with temporal Gaussian distribution and fluence of 5 J/m^2. The laser pulse has 11.5 ps full width at half maximum and is peaked at 10 ps. First, the velocity of molecules is scaled up to 100 ps (time step of 25 fs) to make the sample reach 50 K. Then equilibrium calculation is conducted for another 100 ps to assure the disturbance caused by the velocity scaling is eliminated. Toward the end of equilibration, the ambient gas reaches a pressure of 0.87 MPa. Periodic boundary conditions are imposed to the boundaries in the x and y directions and free boundary conditions to the boundaries in the z direction. Finally after 200 ps, the laser beam heating is applied on the target top surface with volumetric absorption in the material. This incident laser beam is assumed to be absorbed exponentially with an artificial optical absorption depth of 5 nm. A force elimination procedure is applied to eliminate the strong stress wave reflection at the back side of the sample.[19]

The atomic position with evolution and propagation of the primary and secondary shock waves in the background gas is presented in Fig. 1. Additionally, the velocity and pressure distributions are also superimposed in that figure for

[a)]Author to whom correspondence should be addressed. Electronic mail: xwang3@iastate.edu. Tel.: +1-515-294-2085. FAX: +1-515-294-3261.

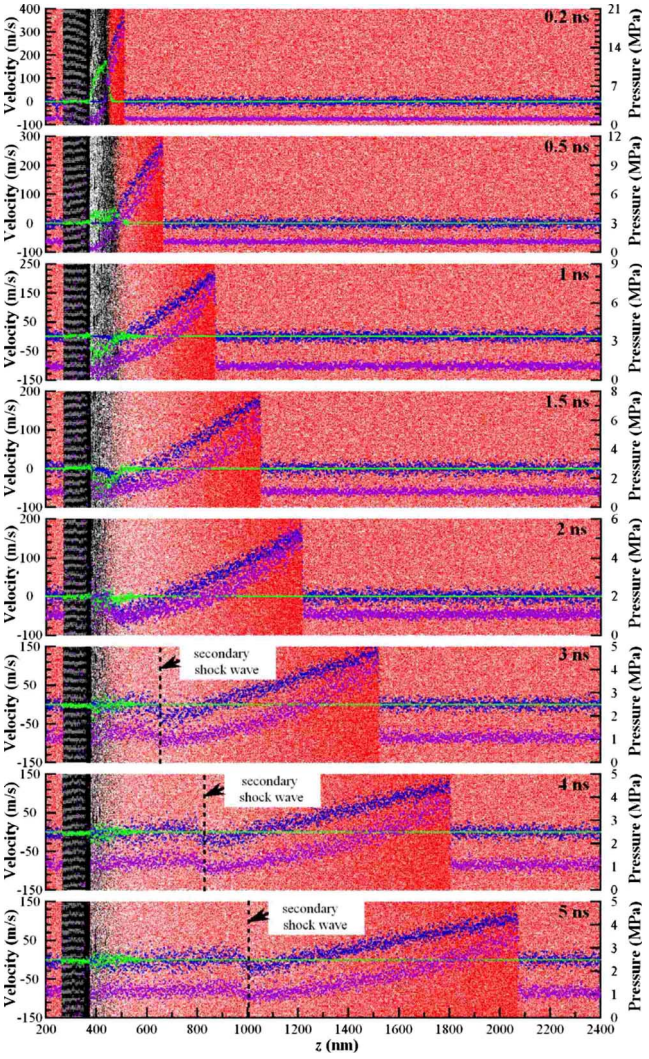

FIG. 1. (Color online) Snapshots of atomic positions combined with the evolution of target and gas velocity, alongside with pressure distribution in the z direction ($E=5$ J/m^2, $\tau=5$ nm, and $P=0.87$ MPa). Green color: target material velocity, blue color: background gas velocity, violet color: pressure, black dots: target atoms, and red dots: ambient gas atoms.

ease of discussion. One of the early stages of the process is shown at 0.2 ns. As it can be seen, the main/primary shock wave front is already formed and is characterized by the high pressure (around 21 MPa) and velocity almost three times the speed of sound (around 390 m/s). An important occurrence starts to happen at 0.5 ns when the velocity of the plume front (green color in Fig. 1) has a substantial decrease. Because of the high ambient gas pressure, the plume undergoes volumetric confinement and in result is being bounced back. The interpretation of this harsh volumetric constraint is the extremely high pressure gradient (the violet curve in Fig. 1) from the compressed ambient gas front to the target surface. While the shock wave front expands further, the plume starts to move backward heading to the surface, which is justified by the large negative velocity of target material at 1 ns. The same trend of the velocity is still visible at 1.5 ns, however with a significant difference in the behavior of the adjacent gas molecules. Due to the backward motion of the plume material, the under-pressure zone created in the vicinity of the plume front (right side) results in the suction of the ambient gas atoms. Therefore, the sucked background gas molecules are being dragged to the target surface, leading to a change in the velocity direction (1.5 ns). At this moment, a negative velocity at the rear of the background gas is observed. At 2 ns a large amount of plume particle cloud is already pushed back and it recombines with the liquid surface. As a result, the velocity of the plume becomes almost zero. In contrast, after being dragged toward the target surface, the ambient gas is reflected from it and begins to propagate in the direction leaving the material surface, ultimately forming the secondary shock wave. At 3 ns, this internal shock wave front is fully discernible, and it is marked (as well as at 4 and 5 ns) in order to improve visual detection since it is rather weak due to the strong dissipation. At 5 ns its velocity does not exceed the value of 50 m/s, meaning it moves almost three times slower in comparison with the main shock wave front. Although in Fig. 1 the secondary shock wave is hard to observe in the atomic configuration due to its weak strength, it is clearly visible in the velocity and pressure distribution enclosed, where at the front of the secondary shockwave, a jump in pressure and velocity is very visible. Similar behavior has been observed in TOF measurements for various plume species analyzed by mass spectroscopy.[9] Our results show good agreement with those scientific output on the velocity and pressure distribution, despite the difference of the inspected materials and disparity in the values.

In order to have a better understanding of the secondary shock wave formation and evolution, it is necessary to analyze its generation from the bulk mass and thermal point of view. For this reason, Fig. 2 is provided to present time sequence of the density and temperature profile along the z direction. At 0.2 and 0.5 ns, as indicated in the figure, there is a density peak at the front of the plume. Due to the high pressure gradient, the plume front is forced to move back toward the target surface. Such backward movement of the plume quickly reduces the density peak, which disappears at 1.5 ns. As marked in figures of 3–5 ns, there is a density jump at the front of the secondary shock wave, which is a direct consequence of the reflected background gas from the target surface. Such density jump justifies the existence of the secondary shock wave. During propagation this internal shock front keeps a distribution width of several mean free paths (5 ns). Likewise, backward motion of the ablated particles was observed in several experiments by TOF spectroscopy or time resolved imaging,[4,7,8] providing considerable close agreement with our result.

In Fig. 2, it is observed that at the front of the main/primary shock wave, there is a significant temperature jump. On the other hand, at the front of the secondary shock wave, the temperature jump is very weak, almost negligible. For the primary shock wave, its front temperature experiences quick dissipation, from 250 K at 0.2 ns to 80 K at 5 ns. In opposite, the temperature of the ambient gas in the rear region (close to the target surface) has very slow dissipation since no stationary low temperature background gas is in contact with it. The secondary shock wave observed in this work is strongly dependent on the laser fluence. We have conducted modeling using different laser fluences for the

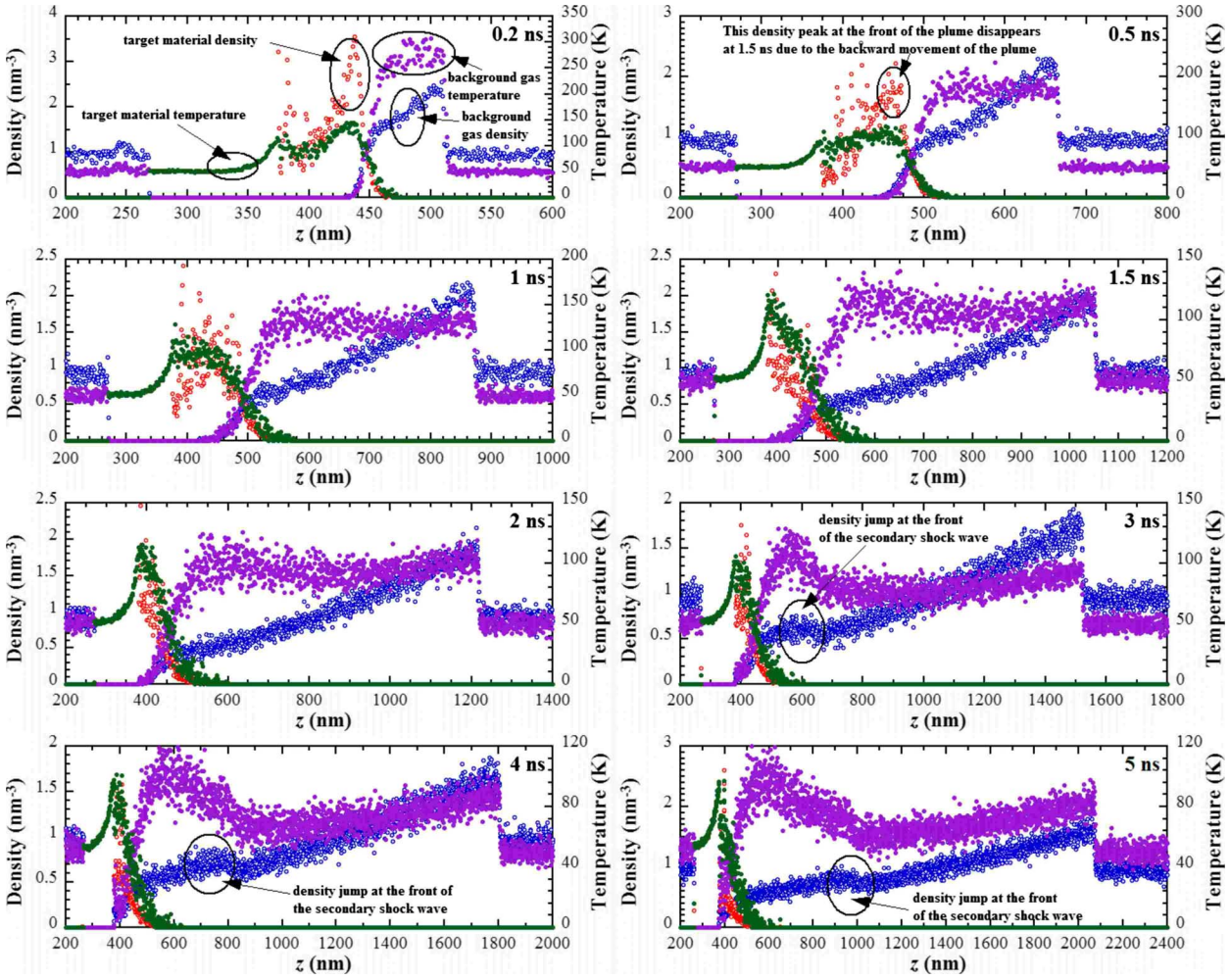

FIG. 2. (Color online) Evolution of density and temperature distribution along the z direction at different times ($E=5$ J/m^2, $\tau=5$ nm, and $P=0.87$ MPa). Red color: target material density, blue color: background gas density, green color: target material temperature, and violet color: background gas temperature.

same pressure and optical absorption depth used in this work. It is found that when the laser fluence is higher (e.g., 7 J/m^2), the secondary shock wave emerges earlier and propagates faster. This is due to the greater plume speed and pressure when the laser fluence is higher. When the laser fluence is reduced to 3 J/m^2, the secondary shock wave is very weak and almost invisible. Therefore, for the laser-material interaction studied in this work, the laser fluence threshold for existence of the secondary shock wave is around 3 J/m^2.

In summary, it is found that the significant pressure gradient inside the shock wave pushed the plume and some of the gas atoms in the rarefield to move back toward the target surface. The plume clusters redeposited on the target surface while the ambient gas atoms were reflected back, leading to the secondary shock wave. Within the secondary shock wave range, the gas has relatively higher pressure, velocity, and density but somewhat less rise in temperature.

Support for this work from the start-up fund of Iowa State University is gratefully acknowledged.

[1] *Laser Ablation of Electronic Materials*, edited by E. Fogarassy and S. Lazare (North-Holland, Amsterdam, 1992).
[2] *Pulsed Laser Deposition of Thin Films*, edited by D. B. Chrisey and G.K. Hubler (Wiley, New York, 1994).
[3] D. B. Geohegan and A. A. Puretzky, Appl. Phys. Lett. **67**, 197 (1995).
[4] J. N. Leboeuf, K. R. Chen, J. M. Donato, D. B. Geohegan, C. L. Liu, A. A. Puretzky, and R. F. Wood, Phys. Plasmas **3**, 2203 (1996).
[5] R. F. Wood, K. R. Chen, J. N. Leboeuf, A. A. Puretzky, and D. B. Geohegan, Phys. Rev. Lett. **79**, 1571 (1997).
[6] M. Han, Y. Gong, J. Zhou, C. Yin, F. Song, N. Muto, T. Takiya, and Y. Iwata, Phys. Lett. A **302**, 182 (2002).
[7] S. S. Harilal, C. V. Bindhu, M. S. Tillack, F. Najmabadi, and A. C. Gaeris, J. Appl. Phys. **93**, 2380 (2003).
[8] S. Singh, M. Argument, Y. Y. Tsui, and R. Fedosejevs, J. Appl. Phys. **98**, 113520 (2005).
[9] A. V. Bulgakov, M. R. Predtechensky, and A. P. Mayorov, Appl. Surf. Sci. **96–98**, 159 (1996).
[10] A. V. Bulgakov and N. M. Bulgakova, J. Phys. D **28**, 1710 (1995).
[11] L. V. Zhigilei, E. Leveugle, B. J. Garrison, Y. G. Yingling, and M. I. Zeifman, Chem. Rev. **103**, 321 (2003).
[12] X. Wang and X. Xu, ASME J. Heat Transfer **124**, 265 (2002).
[13] X. Wang and X. Xu, Int. J. Heat Mass Transfer **46**, 45 (2003).
[14] X. Wang and X. Xu, ASME J. Heat Transfer **125**, 1147 (2003).
[15] X. Wang, J. Phys. D **38**, 1805 (2005).
[16] X. Feng and X. Wang, Phys. Lett. A **369**, 323 (2007).
[17] L. Zhang and X. Wang, Jpn. J. Appl. Phys. **47**, 964 (2008).
[18] M. P. Allen and D. J. Tildesley, *Computer Simulation of Liquids* (Clarendon, Oxford, 1987).
[19] Multiscale Modeling of Materials: Symposium by V. V. Bulatov and L. Kubin (Materials Research Society, 1999), Vol. 538, pp. 491.